Toll-like Receptor 4 Antagonist Restores Vulnerability of Drug-Tolerant Tumor Cells and Prevents Breast Cancer Metastasis and Post-Surgical Relapse

Mou Wang
Sichuan University
Yuejing Wang
Sichuan University
Renhe Liu
Scripps Research Institute
Ruilian Yu
Sichuan Provincial People's Hospital, University of Electronic Science and Technology of China
Tao Gong
Sichuan University
Zhi-Rong Zhang
Sichuan University
Yao Fu (yfu4@scu.edu.cn)
Sichuan University

Research Article

Keywords: Toll like receptor 4, docosahexaenoic acid, cell plasticity, metastasis, postsurgical relapse

Posted Date: March 10th, 2022

DOI: https://doi.org/10.21203/rs.3.rs-1421612/v1

Abstract

Background: Non-mutational mechanisms were recently discovered leading to reversible drug tolerance. Despite the rapid elimination of majority tumor cells, a small sub-population of “drug-tolerant” cells remain viable with lethal drug exposure, which may further lead to resistance or tumor relapse. Several signaling pathways are involved in the local or systemic inflammatory responses contributing to drug-induced phenotypic switch.

Results: In this study, we report Toll like receptor 4 (TLR4)-interacting lipid docosahexaenoic acid (DHA) restores the cytotoxic effect of doxorubicin (DOX) in the lipopolysaccharide-treated breast tumor cell line 4T1, preventing the phenotypic switch to drug-tolerant cells, which significantly reduces primary tumor growth and lung metastasis in both 4T1 orthotopic and experimental metastasis models. Importantly, DHA in combination with DOX delays and inhibits tumor recurrence following surgical removal of the primary tumor. Furthermore, coencapsulation of DHA and DOX in a nanoemulsion significantly prolongs the survival of mice in the postsurgical 4T1 tumor relapse model with significantly reduced systemic toxicity.

Conclusions: The synergistic antitumor, anti-metastasis and anti-recurrence effects of DHA plus DOX combination is likely mediated by attenuating TLR4 activation thus sensitizing tumor cells to standard chemotherapy.

1. Introduction

Clinical studies alarmed the increasing incidence of resistance and metastatic relapses following standard cancer chemotherapy[1, 2]. Among various resistance mechanisms, genetic modifications are a major focus in understanding resistance [3]. Until recently, non-mutational mechanisms leading to drug tolerance have drawn substantial attentions. One of the first clinical evidences pointing to non-mutational mechanism is from the treatment using epidermal growth factor receptor tyrosine kinase inhibitors. After the break of drug treatment, some patients previously showing drug resistance regained sensitivity to the same treatment [4, 5]. This reversible mechanism implied that tumor cells driving their transformation towards the phenotypic state might bypass the original drug-targeted pathway.

The phenotypic changes of cells in response to environmental cues without any genome modification are referred to as cellular plasticity involving several signaling pathways [6]. For example, Marine group identified that under MAPK inhibitor treatment, retinoid X receptor (RXR) signaling pathway is the key driver of the neural crest stem cell state (NCSC) in minimal residual disease [7, 8]. In their study, selective RXR antagonist HX531 was applied to block the RXR signaling which reduced the NCSC-like cell population and improved the cell sensitivity to the treatment [7, 8]. Also, Wnt signaling was shown to modulate drug tolerance through the induction of a Hedgehog-independent pathway in the basal cell carcinoma[9, 10]. The reduction of residual lesions were observed with the blockage of Wnt signaling using either small molecule porcupine inhibitor LGK974 or Wnt receptor LRP6 antibody [9, 10]. A

comparative proteomic approach revealed that cancer cell-derived long pentraxin 3 contributes to melanoma migration and invasion through a Toll-like receptor 4/nuclear factor kappa light chain enhancer of activated B cells (TLR4/NF-κB) signaling pathway, indicating the subpopulation of $MITF^{low}$ melanoma phenotype represents a poteintial therapeutic target [11].

Toll-like receptors (TLRs) are pathogen-pattern recognition receptors and well-known for their roles in host-defense against infections. Emerging evidence also suggests TLRs play a critical role in maintaining tissue homeostasis by regulating the inflammatory and tissue repair responses to injury. Among various TLRs, TLR4 is one of the first receptors to be discovered with crystal structures [12, 13]. Malignant tumor cells can acquire the ectopic expression of TLR4, and once activated, tumor cells may escape the immune surveillance, resulting in further deterioration [14–16]. Moreover, TLR4/NF-κB signaling was implicated in the development of chemoresistance in various cancers as well as to promote cancer cell proliferation, upregulate pro-inflammatory or immunosuppressive cytokines such as tumor necrosis factor alpha (TNF-α), and inhibit the production of an anti-inflammatory cytokine interleukin 10 (IL-10) [17, 18]. Therefore, strategies that can attenuate or block TLR4 activation may provide alternative treatment options for targeting acquired phenotype, modulating cell plasticity, and reversing resistance.

We envision that the multiple non-saturated bonds in the structure of docosahexaenoic acid (DHA) render it a potential TLR4 antagonist for antitumor application while oleic acid (OA) has no TLR4 interaction affinity [19]. In our preliminary study using 4T1 orthotopic tumor bearing mice model, systemic administration of DOX + DHA at a 1:1 molar ratio showed greater primary tumor inhibition than either DOX + OA (1:1 molar ratio) or the standard treatment with DOX-only (Fig. S1). Intriguingly, lung metastasis was dramatically inhibited in the DOX + DHA group whereas DOX + OA group showed no anti-metastasis effect *in vivo* (Fig. S1). This inspired us to explore the anti-metastasis effect and mechanisms of DHA-based therapy for breast cancer treatment. Here we show that lipopolysaccharide (LPS)-stimulated inflammatory responses and distant migration are revised using TLR4-interacting lipid docosahexaenoic acid (DHA) as a chemosensitizer and a potential phenotype modulator. DHA restores the *in vitro* cytotoxic effect of doxorubicin (DOX) in the LPS-treated breast tumor cell line 4T1, significantly inhibits primary tumor growth, reduces lung metastasis and delays post-surgical recurrence in multiple 4T1 mice models.

2. Marerials And Methods

2.1 Reagents

Doxorubicin hydrochloride (DOX) was obtained from Huafeng United Technology (Beijing, China). Docosahexaenoic acid (DHA, C22:6n-3) was purchased from Nu-Chek (Eslyan, MN, USA). Soybean lecithin (S100) was obtained from Lipoid (Ludwigshafen, Germany). Soybean oil was provided by Beiya Medical Oil Co., Ltd. (Tieling, China). Pluronic F68 was kindly offered by BASF (Ludwigshafen, Germany). 3-(4, 5-dimethylthiazol-2-yl)-2, 5-diphenltetrazolium bromide (MTT), lipopolysaccharides (LPS) and 4, 6-

Diamidino-2-phenylindole (DAPI) were purchased from Sigma-Aldrich (St. Louis, Missouri, USA). Other chemicals and reagents were of analytical grade or above.

2.2 Cell culture

RAW264.7 (murine macrophage), DC2.4 (murine dendritic cells), 4T1 (murine breast cancer cells) and 4T1-luc (luciferase tagged murine breast cancer cells) cell lines were obtained from American Type Culture Collection (ATCC, Rockefeller, Maryland, USA). Cells were maintained in Roswell Park Memorial Institute (RPMI) 1640 medium (Hyclone, Logan city, Utah, USA), supplemented with 10% (v/v) fetal bovine serum (Gibco, USA), 100 μg mL^{-1} streptomycin, and 100 U mL^{-1} penicillin (Solarbio, Beijing, China) at 37°C and 5% CO_2. Cells displayed correct phenotypes with expected morphologies and growth curves. Also, mycoplasma detection kit (Shanghai Yise Medical Technology, China) was used to test mycoplasma contamination in the cells.

2.3 Mice

Sprague-Dawley rats (female, 200 ± 20 g) and BALB/c mice (female, 4–6 weeks) were purchased from the Laboratory Animal Center of Sichuan University (Chengdu, China) and maintained under standard housing conditions. All animal experiments and procedures were approved by the Ethics Committee of Sichuan University and performed under the institutional guidelines.

A sample size of 10 was used for animal studies, and a sample size of three was used for cell-based studies. No data or animals were excluded due to being outliers.

2.4 Cell viability assay

4T1 cells were seeded in 96-well plates at 4000 cells per well in 100 μL of RPMI 1640 and incubated at 37°C in a 5% CO_2 atmosphere for 24 h. Cells were pre-stimulated with or without 4 μg mL^{-1} lipopolysaccharide (LPS) for 72 h. To optimize the appropriate proportion, the viability of 4T1 cells treated with or without LPS was studied after incubation with different molar ratios of DHA and DOX at a constant concentration of DOX (1.72 μM) at 37°C for 72 h. Next, the stock solutions of DOX, DHA, and a 1:1 DHA-to-DOX molar ratio mixed solution were spiked in the culture media and incubated for another 72 h. Following treatment with drugs in triplicate, the viability was evaluated by MTT assay. The 50% inhibitory concentration (IC_{50}) was determined by plotting the dose-response curve using GraphPad Prism 5.0.

2.5 Cell apoptosis assay

4T1 cells were pretreated with or without 4 μg mL^{-1} LPS for 72 h, seeded into 12-well plates at a density of 2×10^5 cells each well and allowed to grow to 70–80% confluency. Cells were then incubated with DOX, and DOX + DHA with equivalent concentration of 5.00 μg mL^{-1} DOX and 3.12 μg mL^{-1} DHA in medium. After 4 h of incubation, cells were performed according to the manufacturers' protocols of Annexin V, FITC/PI apoptosis detection kit (Dojindo, AD10) and analyzed using flow cytometry (BD FACS CelestaTM, USA).

2.6 Cell migration assay

Cells were treated with or without 4 μg mL^{-1} LPS for 72 h, seeded into the Culture-Insert 2 Well (ibidi, Germany) and allowed to grow to 90–95% confluency. The insert was then removed, and cells were rinsed with 1 M PBS for three times to create a cell-free gap. Cells were then incubated with DOX (1.00 μg mL^{-1}), DHA (0.57 μg mL^{-1}), and DOX + DHA solution in medium with 1% fetal bovine serum in the wound healing assay. In contrast, cells without any treatment after creating the gap were used as the negative control. The closure rate was determined by visualizing cell migration to the cell-free gap using light microscopy, images were then acquired and analyzed using ImageJ.

2.7 Preparation of DOX/DHA-LNs

First, DOX-oleic acid (DOX-OA) complex was prepared using a co-precipitation method as previously described [20, 21]. Next, 30 mg of DOX-OA (containing about 10 mg of DOX), 604 μL of DHA ethanol solution (10 mg mL^{-1}), 800 mg of lipoid S100, 200 μL of soybean oil, and 1 mL of Pluronic F68 ethanol solution (60 mg mL^{-1}) were dissolved in ethanol in a round-bottom flask. The organic phase was subsequently removed by rotary evaporation (Büchi, Switzerland) under reduced pressure at 37°C until a thin film formed. The dried lipid film was rehydrated in 10 mL of ddH_2O, followed by vigorous vortex, which was then subjected to probe sonication (295 W) for 5 min (JY-92IIN, Ningbo Xinyi, China). The predispersion was passed through a high-pressure homogenizer (EmulsiFlex-C5, AVESTIN, Canada) for 10 cycles at an operating pressure of 90–110 MPa to afford the lipid nanoemulsion (DOX/DHA-LNs) for the concurrent delivery of DOX and DHA.

2.8 Characterization of DOX/DHA-LNs

The particle size and zeta potential were determined by dynamic light scattering (DLS) (Malvern Zetasizer Nano ZS90, UK) at 25°C. The morphology of the obtained nanoemulsion was examined by transmission electron microscopy (H-600, Hitachi, Japan). The entrapment efficiency was determined by ultra-filtration method [22]. To separate free drug from the nanoemulsion suspension, Nanosep® centrifugal filtration devices (Mw cut-off 10 kDa, PALL Life Science, USA) were used. A fixed volume (400 μL) of freshly prepared DOX/DHA-LNs was added to the sample reservoir tube and spun at 6000 rpm at 4°C for 30 min. The collected filtrate in the retentate vial and freshly prepared DOX/DHA-LNs were diluted with 0.12 M HCl in ethanol, and analyzed by fluorescence spectrophotometry using an RF-5301PC spectrofluorophotometer (Shimadzu, Japan) with an excitation wavelength of 472 nm and an emission wavelength of 630 nm. The concentration of DHA was assayed by a high-performance liquid chromatography system (Agilent Technologies 1260 Infinity, USA) consisting of an Agilent ultraviolet detector (G1314C) and a Kromasil reversed-phase C18 column (5 μm, 250 mm × 4.6 mm) (AKZO NOBEL, Sweden). The mobile phase employed for the analysis of DHA consisted of acetonitrile/water containing 0.1% v/v acetic acid (90/10, v/v), and chromatographic elution was maintained at a flow rate of 1.0 mL/min. The detection wavelength was set at 210 nm. The concentration of DHA was determined on the basis of the peak area at a retention time of 9.3 min. The encapsulation efficiency was calculated by the

following formula: Encapsulation efficiency (%) = [1 - (amount of drug in filtrate/amount of drug added)] × 100%.

2.9 *In vitro* drug release

The release profile of DOX from DOX/DHA-LNs was studied using a dialysis setup [23]. Briefly, an appropriate amount DOX/DHA-LNs was transferred to a dialysis tube (MWCO 8000–12000 Da, Millipore, USA) and subjected to dialysis against 50 mL of PBS containing 0.2% w/v Tween 80 to maintain the sink condition and gently shaken at 100 rpm at 37°C with a thermostatted shaker bath (Shenzhen Worldwide Industry, Shenzhen, China). DOX + DHA solution was prepared as a control. During the whole process, the device was protected from light to avoid photodegradation. At given time points, 1 mL aliquot of the medium was collected, and replaced with an equal volume of fresh medium. The concentration of DOX in each sample solution was determined by fluorescence spectrophotometry after dilution with 0.12 M HCl in ethanol.

2.10 Primary tumor growth and spontaneous metastasis

Forty BALB/c mice (female, 6–8 weeks old) were randomly divided into five groups. At day 0, 4T1 cells re-suspended in 0.1 mL PBS were injected into the right mammary gland of BALB/c mice at 1×10^6/mouse. At 14, 17, 20 and 23 d, mice in the five groups were administered via tail vein injection with saline, DOX, DHA, DOX + DHA solution, and DOX/DHA-LNs, respectively, at the equivalent doses of 5.00 mg kg^{-1} DOX and 2.83 mg kg^{-1} DHA. The animal weight and tumor volume were measured twice a week until the end of the experiment. Tumor volume was estimated by measuring the minimum and maximum tumor diameters using the formula: $(\text{minimum diameter})^2 \times (\text{maximum diameter})/2$. At day 42, the mice were sacrificed. Part of primary tumors were digested for flow cytometry analysis (n = 3). The residual primary tumors, lungs, and spleens were collected and washed with cold saline (n = 5). The final tumor weights were measured and the tumor inhibiting rates (TIR) were calculated by the following equation:

$$TIR = (1 - W_{test}/W_{saline}) \times 100\%$$

W_{saline} represented the average tumor weight of saline group and W_{test} referred to that of the tested groups. Then, primary tumors, lungs, and spleens were fixed with 4% paraformaldehyde and imaged with a digital camera. The primary tumor sections were stained by H&E, Ki67, TUNEL, IL-6, and CD34. The spleen sections were stained by H&E, CD4, and CD8. Moreover, the metastatic nodules on the pulmonary tissues were counted, and the lung sections were stained by H&E, F4/80, neutrophil and IL-6. The H&E stained lung sections were subjected to scanning using Pathological section scanner (Pannoramic MIDI, Hungary).

2.11 Experimental metastasis assay

Seventy-five BALB/c mice (female, 6–8 weeks old) were randomly divided into five groups. At day 0, all of them were given 2×10^5 4T1 tumor cells suspended in 0.1 mL PBS by tail vein injection to generate lung metastasis of breast cancer bearing mouse model. At day 4, 7, 10 and 13, mice were systemically given

saline, DOX (5.00 mg kg^{-1}), DHA (2.83 mg kg^{-1}), DOX + DHA and DOX/DHA-LNs. The body weight was recorded. At day 16, five mice were sacrificed in each group (n = 5). The lungs fixed with 4% paraformaldehyde were photographed with a digital camera and the number of lung metastasis nodules was counted. Microscopic metastatic lesions in lungs were revealed after H&E staining of lung tissue sections, where were further subjected to scanning as previously described.

2.12 Postsurgial breast cancer recurrence murine model

BALB/c mice (female, 6–8 weeks) were randomly divided into five groups. First, 1×10^6 4T1-luc cells were inoculated into the right mammary gland of each mouse. When tumors reached ~ 300 mm^3 after approximately 10 days, tumors were surgically removed. Specifically, animals were anaesthetized via intraperitoneal injection of 4% chloral hydrate, and the majority of the tumor mass was removed but left with a layer of surrounding skin with tumor residues to allow tumor relapse. The surgical wound was then closed with sutures. The five groups were subsequently administered via tail vein injection with saline, DOX (5.00 mg/kg), DHA (2.83 mg/kg), DOX + DHA solution and DOX/DHA-LNs at equivalent doses, respectively. Formulations were injected every 3 days for four consecutive times. Meanwhile, the animal weight and tumor volume were measured every 3 days until the end of the experiment. Tumor volume was also estimated by measuring the minimum and maximum tumor diameters using the formula: $(\text{minimum diameter})^2 \times (\text{maximum diameter})/2$. At day 12, three mice from each group were sacrificed. The remaining mice were left for survival study. The tumors, lungs, and spleens were collected and fixed with 4% paraformaldehyde. The tumor sections were stained by H&E, TLR4, Ki67, TUNEL, IL-6, TNF-α and CD34. The spleen sections were stained by H&E, CD4, and CD8.

2.13 *In vivo* bioluminescence and imaging

At day − 1, 0, 4, and 8, mice were anesthetized with 4% chloral hydrate after intraperitoneal injection of D-luciferin potassium salt (150 mg/kg), and imaged using the IVIS® Spectrum in vivo imaging system (Perkin Elmer, USA).

2.14 Patient samples

Human samples were obtained from the Sichuan Provincial People's Hospital. Immunostaining of TLR4 was performed on sections from formalin-fixed paraffin-embedded tissue biopsies obtained from breast cancer patients prior to receiving any chemotherapy. Analysis of human samples was in line with the Institutional Review Board of Sichuan Provincial People's Hospital. Collection of patient samples for scientific purposes was approved by the local ethics committee of Sichuan Provincial People's Hospital (2016-16-1), and written informed consents were obtained.

2.15 Pharmacokinetics and biodistributions *in vivo*

4T1 tumor-bearing mice with tumor size of about 200 mm^3 were fasted for 12 h before experiment and were intravenously given DOX, DOX + DHA, and DOX/DHA-LNs at an equivalent dose of 5.00 mg kg^{-1}

DOX. At each predetermined time point (0.5, 1, 3, 6, 12, 24, and 48 h), three mice were sacrificed, and the blood and tissues (heart, liver, spleen, lung, kidney, and tumor) were collected. Plasma samples were obtained following centrifugation at 6000 rpm for 8 min. All samples were stored at -20°C until analysis. Every tissue sample was accurately weighed, homogenized, and extracted with 0.9% NaCl solution. Homogenized tissue and plasma samples were mixed with four volumes of acetonitrile, vortexed for 10 min and centrifuged at 10000 rpm for 5 min. The supernatants were subjected to LC-MS/MS analysis as previously described[20]. The pharmacokinetic data were generated and analyzed by DAS 3.2.5 (Drug and Statistics, Anhui, China).

2.16 Safety evaluation

Female Sprague Dawley rats (200 ± 20 g) were randomized into 6 groups with 5 rats in each group and fasted for 12 h before administration. Saline, DOX solution (6.00 μg mL^{-1}), DHA solution (3.40 μg mL^{-1}), DOX + DHA, DOX/DHA-LNs and blank LNs were administered intravenously every three days for three consecutive times. The animal weight was recorded every three days. About 0.4 mL of blood samples were collected in centrifuge tubes containing ethylenediamine tetra acetic acid dipotassium salt (EDTA-2K) on either the day before administration or day 3 after administration. White blood cells (WBC) were counted by MEK-6318K automated hematology analyzer (Nijon-kohden, Shinjuku-ku, Japan) as an index of bone marrow suppression. To assess the cardiac and gastrointestinal toxicity, all rats were sacrificed on day 3 after administration, and heart, stomach, duodenum, jejunum, ileum and colon samples were collected. The obtained tissues were fixed with 4% paraformaldehyde for at least 48 h for paraffin sectioning and hematoxylin and eosin (H&E) staining. Degrees of injury such as bleeding, necrosis, hyperaemia, glandular expansion, and decrease in glandular tubes were examined and photographed under light microscope (Axiovert 40CFL, Zeiss, Germany).

2.17 Flow cytometry

Flow cytometry was performed on tumor-associated macrophage (TAM), myeloid-derived suppressor cells (MDSCs), neutrophil and T cells obtained from tumors. Minced mice tumors were digested with 0.5% (w/v) collagenase II solution for 8 h (n = 3). Cells were incubated with anti-CD11b-FITC (BD Pharmagin; 557396) and anti-F4/80-PE (BD Pharmagin; 565410) for TAM. For neutrophil and MDSC staining, anti-CD11b-FITC (BD Pharmagin; 557396), anti-Ly6C-APC (BD Pharmagin; 560595), and anti-Ly6G-PE (BD Pharmagin; 561104) were used. For CD4/CD8 staining, anti-CD4-FITC (BD Pharmagin; 561835) and anti-CD8a-APC (BD Pharmagin; 561093) were used. All stained samples were analyzed by flow cytometry (BD FACS CelestaTM, USA).

2.18 Immunohistochemistry

Routine histological analysis was performed on 4 μm paraformaldehyde-fixed, paraffin-embedded sections. To stain CD8, CD4, IL-6, TLR4, TNF-α, Ki67, TAM, neutrophil and blood vessels, the sections were incubated with anti-mouse CD8 (Abcam, ab203035), CD4 (Abcam, ab221775), IL-6 (Abcam; ab7737), TLR4 (Abcam; ab13556), TNF-α (Abcam, ab6671), Ki67 (Servicebio, GB13030-2), F4/80 (Abcam;

ab1000790), neutrophil (Abcam; ab2557) and CD34 (Abcam; ab187282) at 4 ºC overnight, followed by biotinylated anti-IgG secondary antibodies (ZSGB-BIO). Signal detection was performed using DAB kit (ZSGB-BIO, K135925C) for 2 min at room temperature. Sections were visualized under light microscope (Axiovert 40CFL, Zeiss, Germany).

2.19 TUNEL assay

TUNEL staining was performed according to the manufacturer's instructions (Roche; 11684817910). TUNEL-stained images of were captured using confocal laser scanning microscope (LSM 800, Zeiss, Germany) at 20 × magnification.

2.20 Immunofluorescence

Cells deposited on glass bottom dishes were rinsed with 1× PBS twice, fixed in 4% (w/v) paraformaldehyde for 20 min, permeabilized with 0.1% (w/v) Triton X in PBS, washed and blocked with 1% (w/v) bovine serum albumin (Sigma-Aldrich, USA) in PBS for 60 min. TLR4 antibody (1:100) (Abcam; ab22048) or NF-κB p65 antibody (1:400) (Cell Signaling, D14E12) served as primary reagents. Alexa Fluor 488-conjugated goat anti-rabbit IgG (H + L) (ZSGB-BIO, ZF-0511) and Alexa Flour 488-conjugated goat anti-mouse IgG (H + L) (ZSGB-BIO, ZF-0512) served as secondary reagents. Cells were incubated with primary antibodies in 1% bovine serum albumin in a moist chamber at 4°C overnight and the secondary antibodies (1:400) for 1 h at room temperature (RT) in dark. After DAPI staining, cells were observed with a confocal laser scanning microscope (Leica, Wetzlar, Germany).

Paraffin sections of recurrent tumors were rinsed with 1× PBS three times, permeabilized, blocked, and incubated with antibodies according to the above procedure. TLR4 antibody (1:100) (Abcam; ab22048) served as primary reagents, Cy3-conjugated goat anti-mouse IgG (H + L) (Servicebio; GB21301) served as secondary reagents. After DAPI staining. TLR4 expression of tumor sections were observed with a confocal laser scanning microscope (LSM 800, Zeiss, Germany).

2.21 Statistics analysis

Statistical analyses were performed with Graphpad Prism 6 (GraphPad Software, La Jolla, CA). All data represent mean ± standard deviation (SD). Pairwise comparison testing in experiments with more than two groups was performed using one-way analysis of variance (ANOVA) followed with *post hoc* Tukey test. P values less than 0.05 were considered statistically significant. *$P < 0.05$, **$P < 0.01$, ***$P < 0.001$, ****$P < 0.0001$.

3. Results

3.1 Extensive expression of TLR4 in tumor cells, and tumor-related tissues modulated by LPS and DHA

First, the level of TLR4 expression was characterized via immunofluorescence staining. As a TLR4 agonist, LPS stimulation for 24 h significantly up-regulated the level of TLR4 in 4T1 cells (Fig. S2A and S2B). The healthy lung sections from normal BALB/c mice showed a moderate level of TLR4 expression, which appears comparable to that of lung sections in the absence of metastatic foci from tumor metastasis model mice via immunohistological staining (Fig. S2C). Both the metastatic lung and primary tumor sections obtained from 4T1 orthotopic mammary tumor metastasis model mice showed extensive positive staining of TLR4 (Fig. S2C). Moreover, human breast tumor tissue samples obtained from patients with invasive ductal carcinoma showed that TLR4 was primarily expressed in the ductal epithelial cells (Fig. S2B), indicating a strong correlation between enhanced TLR4 expression and breast cancer cells. Additionally, treatment of 4T1 cells with LPS greatly upregulated the level of membrane associated TLR4, while pretreatment with DHA for a given period of time was proven to attenuate the LPS-driven upregulation of TLR4 expression levels (Fig. 1A and B).

3.2 DHA sensitizes LPS-treated 4T1 cells to standard chemotherapy and the combination of DHA + DOX prevents drug tolerance

LPS is a known TLR4 agonist, which can activate the TLR4/NF-κB signaling pathway and further impact cell proliferation and apoptosis in various cancers [24, 25]. To evaluate the cytotoxic effect of DHA + DOX combination, we studied the cell viability of murine 4T1 cells after treatments of various DHA-to-DOX combinations with or without LPS pre-stimulation. Incubating with 1.72 μM of DOX for 72 h, the presence of DHA significantly enhanced the cytotoxic effect of DOX as compared to DOX-only group (Fig. 1C). Also, varying the molar ratio of DHA-to-DOX from 0.25 to 8 did not result in significant differences in the viability of 4T1 cells with or without LPS pre-stimulation (Fig. 1C). Thereby, a 1:1 DHA-to-DOX molar ratio was selected for the following study.

Incubated for 24 h, DOX-only and DOX + DHA showed a similar concentration-dependent inhibition pattern on 4T1 cells with or without LPS pre-stimulation within an equivalent concentration range of 0.67–21.55 μM DOX (Fig. S2D and S2E). After 72 h-incubation, both DOX-only and DOX + DHA showed a concentration-dependent inhibitory effect on 4T1 cells without LPS pre-stimulation within an equivalent concentration range of 0.07–8.62 μM, while DHA-only showed minimum inhibitory effect within the given concentration range (Fig. 1D). Interestingly, the effect of DHA in the combination was more dramatic at a lower absolute concentration of DOX with a longer period of incubation such as 72 h. 4T1 cells pre-stimulated with LPS for 72 h became insensitive to DOX-only treatment, whereas only the DOX + DHA treated group maintained the concentration-dependent inhibitory effect displaying an IC50 value of 2.914 μM, and no remarkable cytotoxicity was observed in DHA-only treated groups within the concentration range of 0.07–8.62 μM (Fig. 1D). LPS stimulation might contribute to inducing cell phenotypic switch towards a drug-tolerant state, whereas the presence of DHA in the combination appeared to prevent or reverse such switch thus enhancing the cytotoxic effect of DOX.

Next, 4T1 cells were preincubated with or without LPS for 72 h followed by DOX-only or DOX + DHA treatment to evaluate cell apoptosis rate by Annexin V/PI staining. LPS pre-stimulation did not affect the

total apoptosis rate in the control group, whereas with LPS pre-stimulation, 4T1 cells in the DOX-only group showed significantly downregulated apoptosis rate ($P < 0.05$, Fig. 1E), which also indicates a reduced sensitivity to chemotherapy. Interestingly, DOX + DHA treatment showed significantly higher apoptosis rate than DOX-only in LPS pre-stimulated 4T1 cells, which is mainly due to the upregulation of late apoptosis cell proportion (Fig. 1E).

Additionally, pre-stimulation of 4T1 cells with LPS upregulated the level of membrane associated TLR4, and activated the TLR4-mediated signaling pathway with obvious nuclear localization of p65, whereas the presence of DHA attenuated the TLR4 activation mediated by LPS with negligible nuclear translocation of p65 in 4T1 cells (Fig. S2F). Thus, the activation of TLR4-mediated signaling pathway may render 4T1 cells less sensitive to DOX, and the presence of DHA may help restore the chemosensitivity of 4T1 cells by interrupting LPS-mediated TLR4 activation. The effect of DHA in enhancing the chemosensitivity of tumor cells has been reported in cell-line dependent manners. For example, DHA with etoposide exhibited an additive inhibitory effect on brain tumor cells due to the downregulation of events involved in DNA repair and PI3K/MAPK signaling pathways [26]. From our observation, 4T1 cells showed upregulated TLR4 levels after LPS treatment, and obvious nuclear translocation of p65, which is a key indicator of TLR4 activation [27]. The presence of DHA in the combination interrupted the nuclear translocation of p65 thus further attenuating TLR4 activation. This finding suggests the presence of DHA in the combination enhances the chemosensitivity and prevents the phenotypic swtich of LPS-stimulated 4T1 cells possibly via attenuating TLR4-mediated signaling pathway.

3.3 The combination inhibits both 4T1 and macrophage motility *in vitro*

Per the “seed and soil” theory, metastasis is a complex process consisting of primary tumor separation, invasion, and survival in the circulation and lymphatics, as well as growth in a distant organ [28]. To confirm the anti-metastasis effect of DOX + DHA combination, we performed the standard wound closure experiment using both 4T1 and RAW264.7 cells with or without LPS pre-stimulation. Microscopic images were taken at given time points, and wound closure rates were quantified using ImageJ software.

With or without LPS pre-stimulation, treatment of DOX + DHA significantly inhibited the closure of 4T1 compared to the control, DOX-only, or DHA-only groups as seen in the cell monolayer photographed 24 h after stripping (Fig. 1F). No significant differences in the closure rate were observed among control, DOX-only, and DHA-only groups showing an average closure rate of about 90% after 24 h (Fig. 1F). Thus, pretreatment of LPS did not enhance the migration of 4T1 cells in our study. As for RAW264.7, the closure rate showed no significant differences among control, DOX-only, and DHA-only groups with or without LPS stimulation (Fig. 1G), while DOX + DHA combination significantly inhibited the closure rate as compared to the control or single treatment groups. Pre-stimulation RAW264.7 with LPS appeared to increase the motility of cells in the control or DOX + DHA group, whereas LPS pretreatment did not affect cell migration in the DOX-only or DHA-only group (Fig. 1G). This further indicates the inhibition of

migration is likely due to either reduced proliferation or reduced cell motility or both, whereas the DHA-only treated group did not have any proliferation inhibitory effect.

3.4 The combination inhibits 4T1 orthotopic tumor growth and metastasis in mice

To explore the anti-tumor and anti-metastasis effect of the DOX + DHA combination therapy, the 4T1 orthotopic mammary tumor metastasis model, which has often been considered an aggressive triple-negative breast cancer model [29, 30], was established in BALB/c mice and the study was performed as shown in Fig. 2A. In the saline group, primary tumors grew rapidly throughout the experimental period of 4 weeks reaching an average volume of over 1700 mm^3 and an average mass of about 1.3 g (Fig. 2B and C). In comparison, mice treated with free DOX exhibited a similar tumor growth pattern, suggesting limited anti-tumor efficacy of free DOX following the given dosing regimen (Fig. 2B-D). Also, no significant differences in the tumor inhibition effect were observed between saline and DHA-only treated groups (Fig. 2B-D). Thus, DHA-only treatment showed minimum tumor growth inhibition, which was consistent with its cytotoxicity profile *in vitro*. Meanwhile, DOX and DHA were formulated into a pre-established nanoemulsion to afford a co-delivery system, DOX/DHA-LNs, which showed an average size distribution of around 177.6 nm, a zeta potential of -6.28 mV, and over 95% of encapsulation efficiencies for both DOX and DHA (Fig. S3A-D, tables. S1). Compared to the saline group, both DOX + DHA and DOX/DHA-LNs significantly improved the tumor inhibitory effect with 49.01% and 63.13% tumor inhibition rate (TIR), respectively (Fig. 2B-D). The body weight of tumor bearing mice oscillated slightly in all treatment groups (Fig. 2E), indicating relatively low systemic toxicity of these treatments under the given dosing regimen.

To explore the possible mechanisms behind tumor inhibition, tumor bearing mice were sacrificed on day 28 after treatment initiation, and all primary tumors were collected, fixed and sectioned for further analysis. Per histological analysis, most of the tumor cells lost their membrane integrity, showing notable cellular necrosis in tumors treated with either DOX + DHA or DOX/DHA-LNs, whereas no extensive necrosis was observed in tumors treated with DOX-only or DHA-only (Fig. 2F). Regarding proliferation of 4T1 tumor cells *in vivo*, tumor sections displayed extensive Ki67 positive staining in saline, DOX-only, and DHA-only groups (Fig. 2F), and less Ki67 positive staining was observed for DOX + DHA or DOX/DHA-LNs treated groups (Fig. 2F), indicating the proliferation of tumor cells was dramatically suppressed by combination treatments. According to TUNEL staining results, higher cellular apoptosis percentages were observed in DOX + DHA and DOX/DHA-LNs groups than in the other treatment groups (Fig. 2F). Together, above results suggest that the combination of DOX and DHA effectively inhibits primary tumor growth, possibly through the inhibition of tumor proliferation and induction of tumor apoptosis.

Enlarged spleen is sometimes observed in cancer patients undergoing chemotherapy, which marks the negative regulation of the immune system [31, 32]. Mice bearing 4T1 tumor were reported to induce a leukemoid reaction with granulocytosis and splenomegaly [33]. From our observation, among all groups of 4T1 tumor bearing mice, the spleen size of the saline group remained the largest, while DOX-only, and DHA-only groups also showed dramatically increased spleen sizes. However, the spleen volumes of the

two combination groups remained much smaller than the other groups in the cohort (Fig. S3E). A reduction in the spleen size may suggest an anti-inflammatory or a systemic immunomodulating effect of the combination therapy. Per literature, leukemoid reaction caused by the murine 4T1 cells in BALB/c mice is characterized by a significant upregulation of granulocytes in the peripheral blood, which have been critical players in enhancing metastasis [34, 35]. Thereby, the combination therapy may show antimetastasis effect by alleviating granulocytosis in 4T1 tumor bearing mice. Histological analysis of spleen sections further revealed that the areas and shapes of white pulps in the combination groups resembled the morphology of white pulps in the healthy mice, whereas the areas of white pulp in the saline, DOX-only, and DHA-only groups were greatly enlarged compared with healthy mice displaying irregular shapes as well (Fig. S3F). Next, CD4 + and CD8 + T cells of the spleen in tumor-bearing mice declined as compared to normal mice, and DOX-only or DHA-only treatment did not affect the levels of CD4 + and CD8 + T cells compared with the saline group (Fig. S3F). However, in the combination treated groups, the levels of CD4 + T cell populations in the spleen were greatly upregulated (Fig. S3F). Overall, the combination of DOX + DHA was proven highly effective in alleviating splenomegaly and helped maintain the normal tissue morphology of splenic white pulp compartments in 4T1 tumor-bearing mice.

Next, we sought to understand whether the combination therapies would impact orthotopic 4T1 tumor metastasis in mice. As shown in the photographs of the whole lung tissues, the 4T1 tumor-bearing mice treated with saline displayed severe lung metastasis with 21.6 ± 12.01 metastatic nodules (Fig. 2G and H), indicating the successful establishment of 4T1 orthotopic mammary tumor metastasis model. DOX-only treatment showed minimum anti-metastasis effect with an average of 20 ± 7.95 nodules, while DHA-only treatment showed less but not statistically different metastatic nodules of 13.8 ± 3.11. In comparison, DOX + DHA and DOX/DHA-LNs significantly suppressed 4T1 lung metastasis with averages of 2.20 ± 1.64 and 1.20 ± 1.30 metastatic nodules, respectively. Per histological examination, the metastasis lesions exhibited dense cell populations morphologically different from normal lung tissues, and the combination treated groups showed much less lesions than saline, DOX-only, or DHA-only groups (Fig. 2G and H). Hence, the combination therapies of either DOX + DHA or DOX/DHA-LNs suppressed lung metastasis effectively in the 4T1 orthotopic mammary tumor metastasis model.

3.5 The combination suppresses 4T1 lung metastasis in an experimental metastasis model

To further evaluate the anti-metastasis effect of the combination therapies, we established an experimental lung metastasis model in BALB/c mice via tail vein injection of 4T1 cells (Fig. 3A). Multiple metastatic nodules were developed on the lungs of BALB/c mice following saline, DOX-only, or DHA-only treatment (Fig. 3B), indicating DOX and DHA alone showed negligible inhibitory effect against 4T1 lung metastasis following the given dosing regimen. The numbers of lung metastatic nodules in the combination groups of DOX + DHA or DOX/DHA-LNs were significantly fewer than the saline or single treatment groups (Fig. 3B-D). The mice body weight was recorded as an indicator of systemic toxicity and pathologic progression. Only mice in the saline group lost over 20% of their original weight, indicating all treatments have tolerable systemic adverse effects (Fig. 3E). Despite the inhibitory effect against

orthotopic tumor growth, combination therapies of DOX + DHA and DOX/DHA-LNs were again demonstrated to greatly attenuate lung metastasis of 4T1 cells in the experimental metastasis mice model.

3.6 The combination modulates tumor microenvironment against tumor growth and distant metastasis

The combination therapies demonstrated outstanding anti-tumor and anti-metastasis effects *in vivo*, which suggests a potential of the combination in modulating the premetastatic niche to suppress distant tumor metastasis. To explore the possible mechanisms, we first looked at the pharmacokinetic and biodistribution profiles of DOX *in vivo*. Results suggest that the presence of DHA in the combination did not significantly alter the pharmacokinetic and tissue distribution profiles of DOX in mice (table. S2, Fig. S4).

Recent findings report standard chemotherapy induces myeloid-derived suppressor cells (MDSCs) thus attenuating the anticancer efficacy of chemotherapy [36, 37]. MDSCs were divided into two subsets based on the expression patterns of two molecules, *i.e.*, Ly6C and Ly6G. $CD11b^{+}Ly6G^{-}Ly6C^{high}$ cells with monocytic-like morphology are termed monocytic-MDSCs (M-MDSCs), while $CD11b^{+}Ly6G^{+}Ly6C^{low}$ cells with granulocyte-like morphology are termed granulocytic-MDSCs (G-MDSCs)[38]. In tumor tissues, MDSCs differentiate into tumor associated macrophages (TAMs) with tumor-promoting effect [39]. Also, neutrophils in the pre-metastatic lung play a fundamental role in driving breast cancer lung metastasis [40, 41]. We next sought to understand the effects of various treatments on the population of MDSCs, neutrophils, TAMs ($CD11b^{+}F4/80^{+}$), and T-cell populations in primary tumors or lungs. Flow cytometry analysis showed DOX-only treatment upregulated the level of TAMs in the primary tumor as compared to the saline group, whereas treatments containing DHA significantly downregulated the levels of TAMs to the level of the saline control (Fig. S5A). All treatment groups showed comparable levels of M-MDSCs (Fig. S5A). G-MDSCs tended to be upregulated in DOX-only group compared to the saline control, while DHA-containing treatments appeared to restore the level of G-MDSCs to the saline control (Fig. S5A). The level of neutrophil ($CD11b^{+}Ly6G^{+}Ly6C^{+}$) in the combination treated tumors was downregulated as compared to the single treatment (Fig. S5A). All treatments did not affect the level of tumor infiltrating $CD4^{+}$ T cells and $CD8^{+}$ T cells compared with the saline control (Fig. S5B), indicating the combination has no negative regulation for effector T cell populations in the tumor microenvironment. The immunohistological analysis of the lung sections showed the levels of neutrophils in the combination groups were largely downregulated, and the levels of TAMs in the combination groups decreased compared to the saline control (Fig. S5C). Semi-quantitative analysis revealed that the combination significantly reduced the level of interleukin 6 (IL-6) in tumors and lungs compared to the saline, DOX-only and DHA-only treatments (Fig. S5C and S5D). IL-6 has been reported to participate in the differentiation of MDSCs from peripheral blood mononuclear cells (PBMCs) and bone marrow cells [42, 43]. Thus, the downregulation of MDSCs was likely due to the reduction of pro-inflammatory cytokines such as IL-6 [38]. The combination treatment groups displayed significantly less CD34 positive staining of the primary

tumor sections (Fig. S5C and S5E) indicating greatly attenuated tumor-associated vessel formation. Since MDSCs miR-126a has been shown to promote tumor angiogenesis [44], the inhibitory effect of DOX + DHA combination against angiogenesis may result from the downregulation of MDCSs at the tumor site. Taken together, the combination of DOX and DHA decreased the recruitment of MDSCs likely via inhibition of tumor proinflammatory microenvironment, thus resulting in downregulated TAMs, attenuated formation of blood vessels and greater inhibition of primary tumor growth and distant metastasis.

3.7 The combination suppresses postsurgical tumor recurrence and the coencapsulated nanoemulasion prolongs survival

The outstanding antitumor and antimetastasis effects of DOX + DHA combination in the 4T1 orthotopic mice model prompted us to explore whether the combination strategy can prevent postsurgical tumor recurrence. First, 4T1-luc cells were inoculated subcutaneously into the right mammary fat pad of female BALB/c mice to establish the orthotopic 4T1 tumor model. When tumors reached about 300 mm^3, the majority of the primary tumor was surgically resected, and the surgical wound was closed by suture (Fig. 4A). Treatments were maintained similarly as in the antitumor and antimetastasis study (Fig. 4A). According to the *in vivo* imaging results, both DOX + DHA and DOX/DHA-LNs treated groups displayed delayed tumor recurrence compared to the saline group, whereas DOX-only or DHA-only group did not show any delayed tumor recurrence (Fig. 4B). Also, both combination groups showed greater tumor inhibition rates and smaller tumor volumes than in DOX-only or DHA-only groups (Fig. 4C, D). As to the body weight variation, both saline and DHA-only groups showed negligible fluctuations in the average body weight (Fig. 4E). However, all DOX-containing treatments showed gradual weight loss over time, despite that the weight loss appeared to level off after 6 days for DOX/DHA-LNs group (Fig. 4E). This indicates co-encapsulating DOX and DHA in the nanoemulsion might help reduce the systemic toxicity of free DOX to a certain extent.

Next, a survival study was performed to further evaluate the efficacy of the combination therapy in the 4T1 postsurgical relapse model. Compared to the saline group, DOX-only and DHA-only groups showed no obvious effect on prolonging the mean survival of mice (Fig. 4F). Despite the outstanding antitumor efficacy of DOX + DHA in various models, the median survival has been found out to be around 9 days, which is likely due to the systemic toxicity of DOX solution. In comparison, a median survival of over 40 days was observed for DOX/DHA-LNs, further highlighting the importance of co-encapsulating DOX and DHA in a simple nanoemulsion system to improve efficacy and reduce systemic toxicity. Specifically, about 70% of mice remained viable in the DOX/DHA-LNs group within 40 days.

To further understand the therapeutic efficacy in the 4T1 postsurgical relapse model, tumor sections were subjected to immunohistological analysis. H&E stained tumor sections revealed DOX + DHA and DOX/DHA-LNs groups displayed more extensive tumor necrotic regions than the saline, DOX-only or DHA-only group (Fig. S6A). Due to the critical role of angiogenesis in tumor recurrence, assessment of tumor

microvessel was performed by CD34 staining. The CD34 positive staining was significantly downregulated in both DOX + DHA and DOX/DHA-LNs groups compared to that in the saline group (Fig. 5A). Also, significantly less Ki67 positive cells were observed in both DOX + DHA and DOX/DHA-LNs groups (Fig. 5A and C). TUNEL staining was performed to characterize cell apoptosis in the tumor section, which showed extensive positive TUNEL staining with significantly higher percentages in the combination groups (Fig. 5B and D). Taken together, the combination of DOX with DHA appear to significantly inhibit tumor cell proliferation while inducing extensive cell apoptosis and necrosis at the tumor site.

Consistent with the findings in the orthotopic 4T1 tumor metastasis model, the combination therapies also demonstrated dramatic reductions in the spleen size with restored spleen tissue morphology in the postsurgical tumor relapse model (Fig. S6B). However, no significant differences in the level of the CD4 + and CD8 + T cells in the spleen were observed across groups (Fig. S6B), which is likely due to normal host response towards the surgical resection in all groups. Removal of the primary tumor created a surgical wound, which likely resulted in systemic inflammatory responses indicated by the upregulation of pro-inflammatory cytokines such as IL-6 and TNF-α [45]. In our study, pro-inflammatory cytokines, such as IL-6 and TNF-α, were upregulated in the DOX-only groups compared to saline group, but significantly downregulated in DHA-only, DOX + DHA, and DOX/DHA-LNs groups, indicating an antiinflammatory effect of DHA (Fig. 6A and C). To explore whether this antiinflammatory effect is mediated via TLR4, we performed immunofluorescence staining of TLR4 in the tumor sections. Interestingly, DOX-only treatment showed an upregulated level of TLR4 positive staining, and DHA-only appeared to downregulate the level of TLR4 towards the saline level (Fig. 6B and D), whereas the combination groups showed significantly lower levels of TLR4 (Fig. 6B and D). As discussed previously, DHA-only treatment showed no effect in orthotopic tumor inhibition or prevention of metastasis and postsurgical relapse, indicating attenuating TLR4 signaling pathway alone was insufficient to result in any antitumor efficacy. However, it is most likely that attenuating TLR4 signaling pathway might prevent the phenotypic switch of tumor cells upon drug treatment thus sensitizing tumor cells to standard chemotherapy.

3.8 Coadministration of DOX and DHA via nanoemulsion alleviates the systemic toxicity of DOX and demonstrates good tolerability *in vivo*

Bone marrow suppression is one of the most common adverse effects associated with anthracycline-based chemotherapy. The number of white blood cells (WBC) was quantified to investigate the effect of bone marrow suppression in the study. Except for saline, DHA, and blank LNs, all other treatments induced significant reductions in WBC level, indicating a strong bone marrow suppression of DOX-related treatments (Fig. S7A). DOX, DOX + DHA, and DOX/DHA-LNs displayed similar inhibition ratios of (69.3 ± 4.6)%, (72.2 ± 4.2)% and (65.9 ± 4.3)%, respectively, which indicates that the presence of DHA in the combination did not aggravate bone suppression of DOX *in vivo* (Fig. S7B). DHA-only group showed similar inhibition ratio as compared to the saline group (Fig. S7B). Regarding body weight variation, the saline, blank LNs, and DHA groups showed similar changing patterns with slightly increased average body weight over the treatment period (Fig. S7C). In contrast, DOX-only, DOX + DHA and DOX/DHA-LNs

displayed obvious weight loss over the treatment period (Fig. S7C). However, the body weight variation of DOX/DHA-LNs group was significantly less than DOX-only or DOX + DHA groups, indicating that coencapsulating DOX and DHA in LNs may help reduce the systemic toxicity of DOX *in vivo* (Fig. S7C).

The dose-limiting systemic toxicity of DOX remains a serious concern when administered in clinic [46–48]. Thus, we performed histological analysis to further elucidate if the presence of DHA in the combination would impact the cardiotoxicity and gastrointestinal toxicity of DOX. Both DOX-only and DOX + DHA displayed similarly severe cardiotoxicity as observed by hyperemia, myocardial fiber breakage, and necrosis (Fig. S7D). In contrast, the tissue sections from DOX/DHA-LNs treated group did not exhibit obvious signs of cardiotoxicity (Fig. S7D). Both DOX-only and DOX + DHA treated groups displayed intestinal expansion, intestinal villus congestion, intestinal villus atrophy, and a large quantity of cell debris in duodenum, jejunum, and ileum. Although intestinal epithelial cell degeneration was visible in DOX/DHA-LNs treated group, it appeared to be much less obvious as compared with DOX-only and DOX + DHA treated groups (Fig. S7D). Thereby, encapsulating DOX and DHA in LNs via a nanoscale formulation strategy appeared to dramatically reduce DOX-related cardiotoxicity and gastrointestinal injury following systemic administration.

4. Discussions

TLR4-signaling might have either pro- or anti- tumor effect depending on the tumor microenvironment and the different stages of cancer progression which led to drug tolerance and metastasis. TLR4 agonists as immune adjuvants are well demonstrated to enhance tumor inhibition by boosting the systemic immune system [49]. Here, we provided both *in vitro* and *in vivo* proof of TLR4 antagonists as phenotypic modulators for drug-tolerant or metastatic breast cancers. In our study, the systemic administration of DHA with DOX following intravenous injection showed a synergistic inhibitory effect against primary 4T1 breast tumor growth in the orthotopic model as well as extraordinary anti-metastasis effect *in vivo*. Specifically, DHA + DOX showed 3.2-fold higher tumor inhibition rate than DOX-only group in the orthotopic model, whereas DHA-only showed minimum inhibition against primary tumor growth. Moreover, the combination therapy showed significant anti-metastasis effect in both orthotopic and experimental lung metastasis models.

In both 4T1 orthotopic tumor sections and metastatic lung sections, the downregulated levels of IL-6 in the combination groups as compared to the saline control and DOX-only group were likely due to the inactivation of TLR4/NF-κB signaling cascade, which further led to modulation of tumor and metastasis-related immune cells. Studies revealed that upregulation of IL-6 had been correlated with the accumulation of tumor associated macrophages, myeloid-derived suppressor cells (MDSCs) and neutrophils in the orthotopic tumor, which then promoted angiogenesis, tumor relapse and metastasis [50–52]. The combination of DHA with DOX significantly enhanced the chemosensitivity of 4T1 cells, greatly inhibited primary tumor growth, postsurgical relapse, and lung metastasis possibly via attenuation of TLR4 signaling on residual tumor cells, thus resulting in downregulated IL-6 secretion, decreased MDSCs recruitment, and reduced blood vessel formation.

Inflammation has been recognized as a critical contributing factor to induce the invasion or metastasis of breast cancer, and thereby, LPS stimulation was used to generate a 4T1 phenotype with greater viability and invasiveness, which could be considered as drug-tolerant cells. Consistent with *in vivo* findings, *in vitro* cytotoxicity studies showed the superior inhibitory effect of DOX + DHA combination against LPS-stimulated 4T1 cells as compared to DOX alone. Also, the combination efficiently suppressed the migration of 4T1 and RAW264.7 cells in an LPS-independent manner. The presence of DHA was proven to downregulate LPS-stimulated upregulation of membrane-associated TLR4 in 4T1 cells thus interrupting the nuclear translocation of p65 via attenuating TLR4 activation by LPS. Hence, the presence of DHA in the combination significantly enhances the chemosensitivity of LPS-stimulated 4T1 cells and reduces the motility of both 4T1 and RAW264.7 cells possibly via attenuating TLR4-mediated NF-κB signaling pathway.

TLR4 signaling is mediated through either MYD88- or TRIF-dependent pathways during inflammation and antigen presentation [53]. Lipid A is part of the LPS molecule, and the saturated fatty acids acylated on Lipid A are critical in ligand recognition and receptor activation of TLR2 and TLR4 [54–56]. Specifically, LPS binds to CD14 on the lipid raft domain which activates lipid messengers and protein kinase C to further recruit TLR4 via dimerization [57, 58]. Polyunsaturated fatty acids such as DHA were shown to inhibit such LPS-induced dimerization and recruitment of TLR4 into lipid rafts in adenosine triphosphate (ATP) and reactive oxygen species (ROS) dependent manners [54], although upstream molecular signaling response to DHA-TLR4 interaction remains largely unknown. We hypothesized that TLR4 inhibition effect of DHA might attribute to the neutralization of ROS by polyunsaturated fatty acids, and as a result, blocking or attenuating TLR4 signaling would alleviate inflammation thus inhibiting inflammation-associated oncogenesis. This may also explain OA with one double bond showed no effect in attenuating the TLR4 pathway.

Furthermore, the systemic administration of DHA induced minimum vital organ toxicity with no inhibition on white blood cells and hematopoietic functions in rats. Also, co-encapsulating DHA and DOX in a nanoemulsion provides a safe and viable strategy which significantly reduces the cardiotoxicity and gastrointestinal injury induced by free DOX. Overall, a few potential strategies were reported to address cell plasticity such as using epigenetic regulators to reverse cell plasticity, or using intermittent dosing or suppressors targeting the new cell identity[6]. However, some of these therapeutic molecules sufferred from moderate to severe side effects and greatly hindered their applications, despite that some recent studies provided approaches to overcome the intrinsic toxicity and increase therapeutic windows [59, 60]. Our strategy of combining a standard chemotherapeutic drug such as doxorubicin with DHA may represent a highly promising therapeutic scheme to afford rapid clinical translation for the treatment of metastatic breast cancer and postsurgical tumor recurrence.

5. Conclusions

In sum, DHA and DOX combination was proven to enhance the chemosensitivity of 4T1 cells via TLR4-mediated signaling pathway. Besides, the combination could modulate tumor microenvironment to

against 4T1 orthotopic tumor growth, lung metastasis and postsurgical tumor relapse. Moreover, coadministration of DOX and DHA via nanoemulsion alleviated the systemic toxicity of DOX and prolonged survival of recurrent tumor inoculated mice. Overall, our study provides an innovative combination strategy for the management of metastatic breast cancer and postsurgical tumor recurrence.

Declarations

Ethics approval and consent to participate

All animal experiments and procedures were approved by the Ethics Committee of Sichuan University and performed under the institutional guidelines.

Consent for publication

All authors agreed to submit this manuscript.

Availability of data and materials

All data generated or analysed during this study are included in this article and its additional file.

Competing interests

The authors declare no competing fnancial interest. All authors agreed to submit this manuscript.

Funding

This work was funded by National Natural Science Foundation of China (81773654, 81690261, 81503018), Sichuan Provincial Science and Technology Department (2019YJ0019), National Key Research and Development Plan of China (2017YFC1104601), 111 Project (B18035), Sichuan University and Luzhou Fund (2017CDLZ-S32), and Young Investigator Fund of Sichuan Provincial People's Hospital (2015QN06).

Authors' contributions

Yao Fu and Renhe Liu conceived and planned the study. Mou wang and Yuejing Wang carried out the experiments, generated and analyzed data, and wrote the original manuscript. Ruilian Yu provided human breast tissue specimen and contributed to the pathological analysis of tissue sections. Tao Gong and Zhi-Rong Zhang were responsible for funding and equipment support; Yao Fu supervised the entire project, designed experiments, analyzed data and revised the manuscript.

Acknowlegments

We thank that this research was supported by National Natural Science Foundation of China (81773654, 81690261, 81503018), Sichuan Provincial Science and Technology Department (2019YJ0019), National

Key Research and Development Plan of China (2017YFC1104601), 111 Project (B18035), Sichuan University and Luzhou Fund (2017CDLZ-S32), and Young Investigator Fund of Sichuan Provincial People's Hospital (2015QN06).

References

1. Gonzalez-Angulo AM, Morales-Vasquez F, Hortobagyi GN. Overview of resistance to systemic therapy in patients with breast cancer. In Breast Cancer Chemosensitivity. 2007; 608: 1-22. DOI: 10.1007/978-0-387-74039-3_1.
2. Brady SW, McQuerry JA, Qiao Y, Piccolo SR, Shrestha G, Jenkins DF, Layer RM, Pedersen BS, Miller RH, Esch A, et al. Combating subclonal evolution of resistant cancer phenotypes. Nature Communications. 2017; 8. DOI: 10.1038/s41467-017-01174-3.
3. McDonald OG, Wu H, Timp W, Doi A, Feinberg AP. Genome-scale epigenetic reprogramming during epithelial-to-mesenchymal transition. Nat Struct Mol Biol. 2011; 18:867-U821. DOI: 10.1038/nsmb.2084.
4. Kurata T, Tamura K, Kaneda H, Nogami T, Uejima H, Asai G, Nakagawa K, Fukuoka M. Effect of re-treatment with gefitinib ('Iressa', ZD1839) after acquisition of resistance. Ann Oncol. 2004; 15:173-174. DOI: 10.1093/annonc/mdh006.
5. Yano S, Nakataki E, Ohtsuka S, Inayama M, Tomimoto H, Edakuni N, Kakiuchi S, Nishikubo N, Muguruma H, Sone S. Retreatment of lung adenocarcinoma patients with gefitinib who had experienced favorable results from their initial treatment with this selective epidermal growth factor receptor inhibitor: A report of three cases. Oncol Res. 2005; 15:107-111. DOI: 10.3727/096504005775082020.
6. Boumahdi S, de Sauvage FJ. The great escape: tumour cell plasticity in resistance to targeted therapy. Nature Reviews Drug Discovery. 2019:1-18. DOI: 10.1038/s41573-019-0044-1.
7. Rambow F, Rogiers A, Marin-Bejar O, Aibar S, Femel J, Dewaele M, Karras P, Brown D, Chang YH, Debiec-Rychter M, et al. Toward Minimal Residual Disease-Directed Therapy in Melanoma. Cell. 2018; 174:843-+. DOI: 10.1016/j.cell.2018.06.025.
8. Su Y, Wei W, Robert L, Xue M, Tsoi J, Garcia-Diaz A, Moreno BH, Kim J, Ng RH, Lee JW, et al. Single-cell analysis resolves the cell state transition and signaling dynamics associated with melanoma drug-induced resistance. Proc Natl Acad Sci U S A. 2017; 114:13679-13684. DOI: 10.1073/pnas.1712064115.
9. Biehs B, Dijkgraaf GJP, Piskol R, Alicke B, Boumahdi S, Peale F, Gould SE, de Sauvage FJ. A cell identity switch allows residual BCC to survive Hedgehog pathway inhibition. Nature. 2018; 562:429-+. DOI: 10.1038/s41586-018-0596-y.
10. Sanchez-Danes A, Larsimont J-C, Liagre M, Munoz-Couselo E, Lapouge G, Brisebarre A, Dubois C, Suppa M, Sukumaran V, del Marmol V, et al. A slow-cycling LGR5 tumour population mediates basal cell carcinoma relapse after therapy. Nature. 2018; 562:434-+. DOI: 10.1038/s41586-018-0603-3.

11. Rathore M, Girard C, Ohanna M, Tichet M, Ben Jouira R, Garcia E, Larbret F, Gesson M, Audebert S, Lacour JP, et al. Cancer cell-derived long pentraxin 3 (PTX3) promotes melanoma migration through a toll-like receptor 4 (TLR4)/NF-kappa B signaling pathway. Oncogene. 2019; 38:5873-5889. DOI: 10.1038/s41388-019-0848-9.
12. Matsushima N, Miyashita H, Enkhbayar P, Kretsinger RH. Comparative Geometrical Analysis of Leucine-Rich Repeat Structures in the Nod-Like and Toll-Like Receptors in Vertebrate Innate Immunity. Biomolecules. 2015; 5:1955-1978. DOI: 10.3390/biom5031955.
13. Kim HM, Park BS, Kim J-I, Kim SE, Lee J, Oh SC, Enkhbayar P, Matsushima N, Lee H, Yoo OJ, Lee J-O. Crystal structure of the TLR4-MD-2 complex with bound endotoxin antagonist eritoran. Cell. 2007; 130:906-917. DOI: 10.1016/j.cell.2007.08.002.
14. Sheyhidin I, Nabi G, Hasim A, Zhang R-P, Ainiwaer J, Ma H, Wang H. Overexpression of TLR3, TLR4, TLR7 and TLR9 in esophageal squamous cell carcinoma. World J Gastroenterol. 2011; 17:3745-3751. DOI: 10.3748/wjg.v17.i32.3745.
15. Dickinson SE, Wondrak GT. TLR4 in skin cancer: From molecular mechanisms to clinical interventions. Mol Carcinog. 2019; 58:1086-1093. DOI: 10.1002/mc.23016.
16. Ran S, Bhattarai N, Patel R, Volk-Draper L. TLR4-Induced Inflammation Is a Key Promoter of Tumor Growth, Vascularization, and Metastasis. In *Translational Studies on Inflammation.* IntechOpen; 2019. DOI: 10.5772/intechopen.85195.
17. Zhang YT, Wang Y, Yuan JL, Qin WJ, Liu F, Wang FL, Zhang G, Yang XJ. Toll-like receptor 4 ligation confers chemoresistance to docetaxel on PC-3 human prostate cancer cells. Cell Biology And Toxicology. 2012; 28:269-277. DOI: 10.1007/s10565-012-9221-2.
18. Zu YK, Ping W, Deng TR, Zhang N, Fu XN, Sun W. Lipopolysaccharide-induced toll-like receptor 4 signaling in esophageal squamous cell carcinoma promotes tumor proliferation and regulates inflammatory cytokines expression. Diseases of the Esophagus. 2017; 30. DOI: 10.1111/dote.12466.
19. Hwang DH, Kim J-A, Lee JY. Mechanisms for the activation of Toll-like receptor 2/4 by saturated fatty acids and inhibition by docosahexaenoic acid. Eur J Pharmacol. 2016; 785:24-35. DOI: 10.1016/j.ejphar.2016.04.024.
20. Cao X, Luo JW, Gong T, Zhang ZR, Sun X, Fu Y. Coencapsulated Doxorubicin and Bromotetrandrine Lipid Nanoemulsions in Reversing Multidrug Resistance in Breast Cancer in Vitro and in Vivo. Molecular Pharmaceutics. 2015; 12:274-286. DOI: 10.1021/mp500637b.
21. Zhang XM, Sun X, Li JL, Zhang XN, Gong T, Zhang ZR. Lipid nanoemulsions loaded with doxorubicin-oleic acid ionic complex: characterization, in vitro and in vivo studies. Pharmazie. 2011; 66:496-505. DOI: 10.1691/ph.2011.0379.
22. Ma P, Dong XW, Swadley CL, Gupte A, Leggas M, Ledebur HC, Mumper RJ. Development of Idarubicin and Doxorubicin Solid Lipid Nanoparticles to Overcome Pgp-Mediated Multiple Drug Resistance in Leukemia. Journal of Biomedical Nanotechnology. 2009; 5:151-161. DOI: 10.1166/jbn.2009.1021.
23. Zhang J, Chen XG, Li YY, Liu CS. Self-assembled nanoparticles based on hydrophobically modified chitosan as carriers for doxorubicin. Nanomedicine-Nanotechnology Biology and Medicine. 2007;

3:258-265. DOI: 10.1016/j.nano.2007.08.002.

24. O'Neill LAJ, Golenbock D, Bowie AG. The history of Toll-like receptors - redefining innate immunity. Nature Reviews Immunology. 2013; 13:453-460. DOI: 10.1038/nri3446.
25. Aggarwal BB, Sung B. NF-kappa B in Cancer: A Matter of Life and Death. Cancer Discovery. 2011; 1:469-471. DOI: 10.1158/2159-8290.cd-11-0260.
26. Wang F, Bhat K, Doucette M, Zhou S, Gu Y, Law B, Liu X, Wong ET, Kang JX, Hsieh TC, et al. Docosahexaenoic Acid (DHA) Sensitizes Brain Tumor Cells to Etoposide-Induced Apoptosis. Current Molecular Medicine. 2011; 11:503-511. DOI: 10.2174/156652411796268740.
27. Yuan X, Zhou Y, Wang W, Li J, Xie G, Zhao Y, Xu D, Shen L. Activation of TLR4 signaling promotes gastric cancer progression by inducing mitochondrial ROS production. Cell Death & Disease. 2013; 4. DOI: ARTN e79410.1038/cddis.2013.334.
28. Hunter KW, Crawford NP, Alsarraj J. Mechanisms of metastasis. Breast Cancer Research. 2008; 10 Suppl 1:S2. DOI: 10.1186/bcr1988.
29. Kaur P, Nagaraja GM, Zheng H, Gizachew D, Galukande M, Krishnan S, Asea A. A mouse model for triple-negative breast cancer tumor-initiating cells (TNBC-TICs) exhibits similar aggressive phenotype to the human disease. BMC Cancer. 2012; 12:120. DOI: 10.1186/1471-2407-12-120.
30. Bourgeois-Daigneault M-C, Roy DG, Aitken AS, El Sayes N, Martin NT, Varette O, Falls T, St-Germain LE, Pelin A, Lichty BD. Neoadjuvant oncolytic virotherapy before surgery sensitizes triple-negative breast cancer to immune checkpoint therapy. Sci Transl Med. 2018; 10:eaao1641. DOI: 10.1126/scitranslmed.aao1641.
31. Brar SS, Seevaratnam R, Cardoso R, Law C, Helyer L, Coburn N. A systematic review of spleen and pancreas preservation in extended lymphadenectomy for gastric cancer. Gastric Cancer. 2012; 15:S89-S99. DOI: 10.1007/s10120-011-0087-4.
32. Radoja S, Rao TD, Hillman D, Frey AB. Mice bearing late-stage tumors have normal functional systemic T cell responses in vitro and in vivo. Journal of Immunology. 2000; 164:2619-2628. DOI: DOI 10.4049/jimmunol.164.5.2619.
33. duPre SA, Hunter KW, Jr. Murine mammary carcinoma 4T1 induces a leukemoid reaction with splenomegaly: Association with tumor-derived growth factors. Exp Mol Pathol. 2007; 82:12-24. DOI: 10.1016/j.yexmp.2006.06.007.
34. Tabariès S, Ouellet V, Hsu BE, Annis MG, Rose AA, Meunier L, Carmona E, Tam CE, Mes-Masson A-M, Siegel PM. Granulocytic immune infiltrates are essential for the efficient formation of breast cancer liver metastases. Breast Cancer Res. 2015; 17:45. DOI: 10.1186/s13058-015-0558-3.
35. Al-Mahmood S, Sapiezynski J, Garbuzenko OB, Minko T. Metastatic and triple-negative breast cancer: challenges and treatment options. Drug Delivery And Translational Research. 2018; 8:1483-1507. DOI: 10.1007/s13346-018-0551-3.
36. Bruchard M, Mignot G, Derangere V, Chalmin F, Chevriaux A, Vegran F, Boireau W, Simon B, Ryffel B, Connat JL, et al. Chemotherapy-triggered cathepsin B release in myeloid-derived suppressor cells

activates the Nlrp3 inflammasome and promotes tumor growth. Nature Medicine. 2013; 19:57-64. DOI: 10.1038/nm.2999.

37. Limagne E, Euvrard R, Thibaudin M, Rebe C, Derangere V, Chevriaux A, Boidot R, Vegran F, Bonnefoy N, Vincent J, et al. Accumulation of MDSC and Th17 Cells in Patients with Metastatic Colorectal Cancer Predicts the Efficacy of a FOLFOX-Bevacizumab Drug Treatment Regimen. Cancer Research. 2016; 76:5241-5252. DOI: 10.1158/0008-5472.CAN-15-3164.
38. Condamine T, Gabrilovich DI. Molecular mechanisms regulating myeloid-derived suppressor cell differentiation and function. Trends In Immunology. 2011; 32:19-25. DOI: 10.1016/j.it.2010.10.002.
39. Kusmartsev S, Gabrilovich DI. STAT1 signaling regulates tumor-associated macrophage-mediated T cell deletion. Journal Of Immunology. 2005; 174:4880-4891. DOI: 10.4049/jimmunol.174.8.4880.
40. Spiegel A, Brooks MW, Houshyar S, Reinhardt F, Ardolino M, Fessler E, Chen MB, Krall JA, DeCock J, Zervantonakis IK, et al. Neutrophils Suppress Intraluminal NK Cell-Mediated Tumor Cell Clearance and Enhance Extravasation of Disseminated Carcinoma Cells. Cancer Discovery. 2016; 6:630-649. DOI: 10.1158/2159-8290.CD-15-1157.
41. Wculek SK, Malanchi I. Neutrophils support lung colonization of metastasis-initiating breast cancer cells. Nature. 2015; 528:413-417. DOI: 10.1038/nature16140.
42. Marigo I, Bosio E, Solito S, Mesa C, Fernandez A, Dolcetti L, Ugel S, Sonda N, Bicciato S, Falisi E, et al. Tumor-Induced Tolerance and Immune Suppression Depend on the C/EBP beta Transcription Factor. Immunity. 2010; 32:790-802. DOI: 10.1016/j.immuni.2010.05.010.
43. Lechner MG, Liebertz DJ, Epstein AL. Characterization of Cytokine-Induced Myeloid-Derived Suppressor Cells from Normal Human Peripheral Blood Mononuclear Cells. Journal of Immunology. 2010; 185:2273-2284. DOI: 10.4049/jimmunol.1000901.
44. Deng Z, Rong Y, Teng Y, Zhuang X, Samykutty A, Mu J, Zhang L, Cao P, Yan J, Miller D, Zhang HG. Exosomes miR-126a released from MDSC induced by DOX treatment promotes lung metastasis. Oncogene. 2017; 36:639-651. DOI: 10.1038/onc.2016.229.
45. Krall JA, Reinhardt F, Mercury OA, Pattabiraman DR, Brooks MW, Dougan M, Lambert AW, Bierie B, Ploegh HL, Dougan SK, Weinberg RA. The systemic response to surgery triggers the outgrowth of distant immune-controlled tumors in mouse models of dormancy. Sci Transl Med. 2018; 10. DOI: 10.1126/scitranslmed.aan3464.
46. Smith LA, Cornelius VR, Plummer CJ, Levitt G, Verrill M, Canney P, Jones A. Cardiotoxicity of anthracycline agents for the treatment of cancer: Systematic review and meta-analysis of randomised controlled trials. Bmc Cancer. 2010; 10:337. DOI: Artn 33710.1186/1471-2407-10-337.
47. Shuhendler AJ, Prasad P, Zhang RX, Amini MA, Sun M, Liu PP, Bristow RG, Rauth AM, Wu XY. Synergistic Nanoparticulate Drug Combination Overcomes Multidrug Resistance, Increases Efficacy, and Reduces Cardiotoxicity in a Nonimmunocompromised Breast Tumor Model. Molecular Pharmaceutics. 2014; 11:2659-2674. DOI: 10.1021/mp5000093c.
48. Kim JE, Yoon IS, Cho HJ, Kim DH, Choi YH, Kim DD. Emulsion-based colloidal nanosystems for oral delivery of doxorubicin: Improved intestinal paracellular absorption and alleviated cardiotoxicity.

International Journal Of Pharmaceutics. 2014; 464:117-126. DOI: 10.1016/j.ijpharm.2014.01.016.

49. Traini G, Ruiz-de-Angulo A, Blanco-Canosa JB, Zamacola Bascarán K, Molinaro A, Silipo A, Escors D, Mareque-Rivas JC. Cancer Immunotherapy of TLR4 Agonist–Antigen Constructs Enhanced with Pathogen-Mimicking Magnetite Nanoparticles and Checkpoint Blockade of PD-L1. Small. 2019; 15:1803993. DOI: 10.1002/smll.201803993.
50. Bergenfelz C, Gaber A, Allaoui R, Mehmeti M, Jirström K, Leanderson T, Leandersson K. S100A9 expressed in ER− PgR− breast cancers induces inflammatory cytokines and is associated with an impaired overall survival. Br J Cancer. 2015; 113:1234. DOI: 10.1038/bjc.2015.346.
51. Lowe JM, Menendez D, Bushel PR, Shatz M, Kirk EL, Troester MA, Garantziotis S, Fessler MB, Resnick MA. p53 and NF-κB coregulate proinflammatory gene responses in human macrophages. Cancer Res. 2014; 74:2182-2192. DOI: 10.1158/0008-5472.CAN-13-1070.
52. Gonda K, Shibata M, Ohtake T, Matsumoto Y, Tachibana K, Abe N, Ohto H, Sakurai K, Takenoshita S. Myeloid-derived suppressor cells are increased and correlated with type 2 immune responses, malnutrition, inflammation, and poor prognosis in patients with breast cancer. Oncol Lett. 2017; 14:1766-1774. DOI: 10.3892/ol.2017.6305.
53. Premkumar V, Dey M, Dorn R, Raskin I. MyD88-dependent and independent pathways of Toll-Like Receptors are engaged in biological activity of Triptolide in ligand-stimulated macrophages. BMC chemical biology. 2010; 10:3-3. DOI: 10.1186/1472-6769-10-3.
54. Wong SW, Kwon M-J, Choi AMK, Kim H-P, Nakahira K, Hwang DH. Fatty Acids Modulate Toll-like Receptor 4 Activation through Regulation of Receptor Dimerization and Recruitment into Lipid Rafts in a Reactive Oxygen Species-dependent Manner. Journal of Biological Chemistry. 2009; 284:27384-27392. DOI: 10.1074/jbc.M109.044065.
55. Akira S, Takeda K, Kaisho T. Toll-like receptors: critical proteins linking innate and acquired immunity. Nature Immunology. 2001; 2:675-680. DOI: 10.1038/90609.
56. Takeuchi O, Hoshino K, Kawai T, Sanjo H, Takada H, Ogawa T, Takeda K, Akira S. Differential roles of TLR2 and TLR4 in recognition of gram-negative and gram-positive bacterial cell wall components. Immunity. 1999; 11:443-451. DOI: 10.1016/s1074-7613(00)80119-3.
57. Erridge C, Kennedy S, Spickett CM, Webb DJ. Oxidized phospholipid inhibition of Toll-like receptor (TLR) signaling is restricted to TLR2 and TLR4 - Roles for CD14, LPS-binding protein, and MD2 as targets for specificity of inhibition. Journal of Biological Chemistry. 2008; 283:24748-24759. DOI: 10.1074/jbc.M800352200.
58. Park BS, Song DH, Kim HM, Choi B-S, Lee H, Lee J-O. The structural basis of lipopolysaccharide recognition by the TLR4-MD-2 complex. Nature. 2009; 458:1191-U1130. DOI: 10.1038/nature07830.
59. Watanabe M, Kakuta H. Retinoid X receptor antagonists. International journal of molecular sciences. 2018; 19:2354. DOI: 10.3390/ijms19082354.
60. Yin S, Luo J, Qian A, Yu W, Hu H. LE135, a retinoid acid receptor antagonist, produces pain through direct activation of TRP channels. Br J Pharmacol. 2014; 171:1510-1520. DOI: 10.1111/bph.12543.

Figures

Figure 1

Effect of DHA on TLR4 expression, cytotoxicity and cell migration *in vitro*. **A** Representative confocal images of TLR4 expression patterns in murine 4T1 cells after treated with 10 μM DHA for 24 h followed by 4 μg mL^{-1} LPS stimulation. Scale bar = 10 μm. **B** Fluorescence intensity per cell of TLR4 on 4T1 cells is analyzed by ImageJ. **C** At a constant DOX concentration of 1.72 μM, dose-response histograms of 4T1 cells without (left) or with (right) 4 μg mL^{-1} LPS pre-stimulation for 72 h against different molar ratios of DHA and DOX for 72 h. **D** Dose-response curves of 4T1 cells untreated (left) or treated (right) with 4 μg mL^{-1} LPS pre-stimulation for 72 h against DOX, DHA, and DOX + DHA for 72 h. **E** Apoptosis rate (left) and late apoptosis rate (right) of 4T1 cells untreated or treated with 4 μg mL^{-1} LPS pre-stimulation for 72 h against DOX, and DOX+DHA with equivalent concentration of 5.00 μg mL^{-1} DOX and 3.12 μg mL^{-1} DHA for 4 h. **F** and **G** Representative images of 4T1 (left) and RAW264.7 (right) pre-stimulation with 4 μg mL^{-1} LPS for 72 h or not were taken by phase contrast microscope before and after treatment with 1.00 μg mL^{-1} DOX or 0.57 μg mL^{-1} DHA. Closure rates were obtained by ImageJ software (below). Data represent means ± SD (n = 3). P values were determined by one-way ANOVA with *post hoc* Tukey test and represented using* P <0.05, ** P < 0.01, *** P < 0.001, and **** P < 0.0001. n.s., not significant.

Figure 2

Tumor inhibitory effect and anti-metastasis effect *in vivo*. **A** Design and timeline of animal experiment to test anti-metastasis and survival *in vivo*. iv., intravenous. **B** Photographs of tumors. **C** The tumor weights at the end of the experiment. **D** The tumor volumes after treated with saline, DOX, DHA, DOX + DHA, and DOX/DHA-LNs for four times with equivalent doses of 5.00 mg kg^{-1} DOX and 2.83 mg kg^{-1} DHA. **E** The variation profiles of body weights. **F** Representative images of tumor sections stained for hematoxylin and eosin (H&E), Ki67 and TUNEL, respectively. Scale bar = 200 μm. Data represent mean ± SD (n = 5). **G** Representative images and histopathologic examination of lungs from 4T1 tumor-bearing mice after treated with saline, DOX, DHA, DOX + DHA, and DOX/DHA-LNs for four times with 5.00 mg kg^{-1} DOX and 2.83 mg kg^{-1} DHA. **H** Quantitative analysis of the pulmonary metastatic nodules of the lungs. Data represent mean ± SD (n = 5). P values were determined by one-way ANOVA with *post hoc* Tukey test and represented using* P <0.05, ** P < 0.01, *** P < 0.001, and **** P < 0.0001.

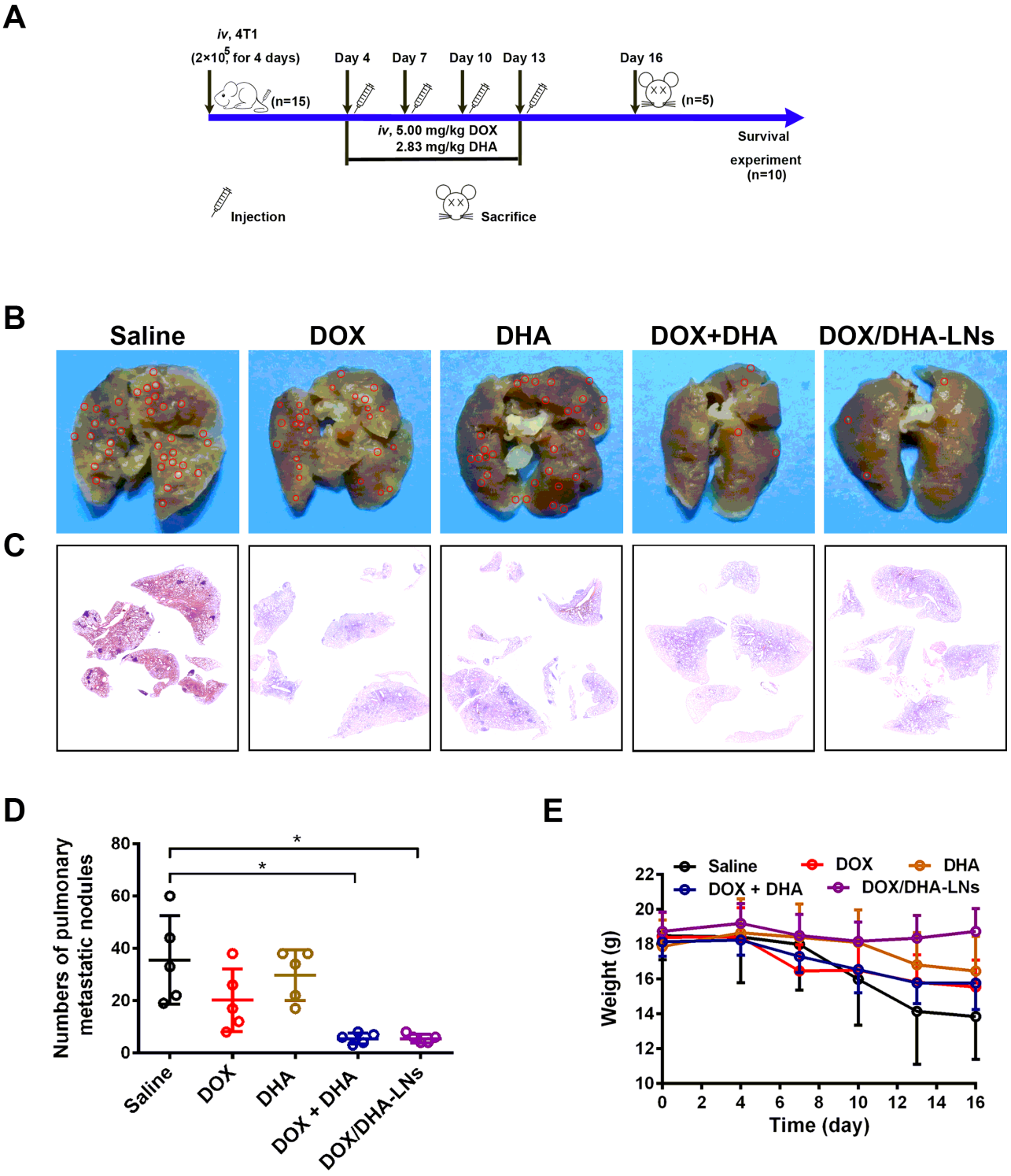

Figure 3

Anti-metastasis in the 4T1 experimental lung metastasis model. **A** Design and timeline of animal experiment to test anti-metastasis and survival *in vivo*. *iv.*, intravenous. **B** Representative images of collected lungs. **C** Representative histological lung sections stained with H&E. **D** Quantitative analysis of pulmonary metastatic nodules. **E** Body weight changes after treated with saline, DOX, DHA, DOX + DHA, and DOX/DHA-LNs for four times with 5.00 mg kg^{-1} DOX and 2.83 mg kg^{-1} DHA. Red circles indicate the

metastatic nodules. Data represent mean ± SD (n = 5). P values were determined by one-way ANOVA with *post hoc* Tukey test and represented using*P<0.05 and **P< 0.01.

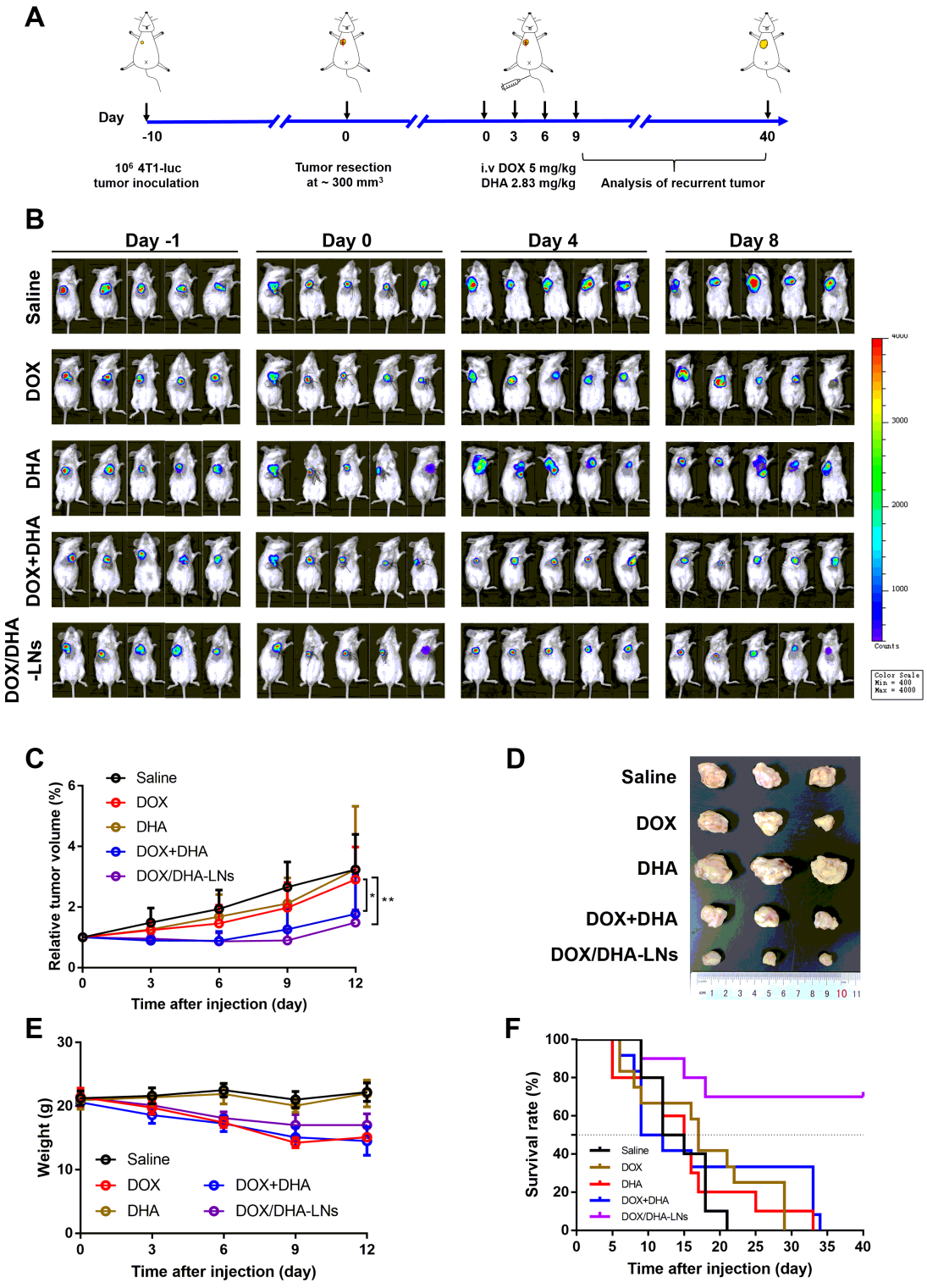

Figure 4

Anti-tumor effect in the post-surgical relapse 4T1-luc tumor model in mice. **A** Surgical and treatment procedures of 4T1-luc tumor relapse model. *iv.*, intravenous. **B** The relative tumor volumes after treated

with saline, DOX, DHA, DOX + DHA, and DOX/DHA-LNs for four times with equivalent doses of 5.00 mg kg^{-1} DOX and 2.83 mg kg^{-1} DHA. **C** Photographs of tumors collected from mice were treated as indicated after 12 days. **D** The variation profiles of body weights. **E** Survival curves of the treatment groups up to 40 days after administration (n = 10). **F** *In vivo* IVIS images of 4T1-luc tumors after resection of the primary tumor. P values were determined by one-way ANOVA with *post hoc* Tukey test and represented using* $P < 0.05$ and ** $P < 0.01$.

Figure 5

Histological analysis of tumor sections in the post-surgical relapse 4T1-luc tumor model. **A** Representative images of tumor sections stained for CD34 and Ki67, scale bar = 50 μm. **B** TUNEL assay on the recurrence tumor sections, scale bar = 100 μm. **C** Proportion of Ki67 positive cells is analyzed using Image pro plus, and is calculated as follows: $N_K/N_B \times 100\%$, N_K, number of Ki67-stained cells; $N_{B,}$ number of blue-stained cells. **D** Percentage of apoptotic cells is determined as follows: $N_T/ (N_B+N_T-N_C) \times 100\%$, N_T, number of TUNEL-stained cells; $N_{B,}$ number of blue-stained cells; N_C, number of cyan-stained cells. P values were determined by one-way ANOVA with *post hoc* Tukey test and represented using* $P < 0.05$, ** $P < 0.01$ and *** $P < 0.001$.

Figure 6

Inflammatory cytokines and TLR4 levels in post-surgical relapse 4T1-luc tumor model. **A** Immunohistochemical analysis of IL-6 and TNF-α, scale bar = 50 μm. **B** TLR4 expression on the 4T1-luc tumor sections was detected by immunofluorescence staining, scale bar = 50 μm. **C** Semi-quantitative analysis of IL-6 and TNF-α in 4T1-luc relapse tumor model. **D** Fluorescence intensity per cell of TLR4 expression on the tumor sections was obtained by Image pro plus. P values were determined by one-way ANOVA with *post hoc* Tukey test and represented using *** $P < 0.001$.

Supplementary Files

This is a list of supplementary files associated with this preprint. Click to download.

- Graphicalabstract.png
- SupplementarymaterialJournalofNanobiotechnology.docx